Study of Solar Wind and Interplanetary Magnetic Field Features Associated with Geomagnetic Storms: The Cross Wavelet Approach

Sujan Prasad Gautam[1], Ashok Silwal[2*], Prakash Poudel[2], Monika Karki[3], Binod Adhikari[4], Narayan Prasad Chapagain[3]

[1]Central Department of Physics, Tribhuvan University, Kathmandu, Nepal

[2]Department of Physics, Patan Multiple Campus, Tribhuvan University, Lalitpur, Nepal

[3]Department of Physics, Amrit Campus, Tribhuvan University, Kathmandu, Nepal

[4]St. Xavier's College, Maitighar, Kathmandu, Nepal

*Corresponding author: ashoksilwal0@gmail.com

Abstract

Researchers have studied the interplanetary magnetic field (IMF) and solar-wind (SW) parameters that influence the development of geomagnetic storms for more than a decade. This study utilised newly developed tools for investigating the association between solar and interplanetary plasma parameters along with geomagnetic (GM) indices during two different geomagnetic storms of varying intensity that occurred on 20 November 2003 (SYM-H = -490 nT) and 22 June 2015 (SYM-H = -139 nT). As the largest storm in Solar Cycle (SC)-23 and the second largest in SC-24, these events were deliberately chosen to represent extreme space weather activity. The study of these severe geomagnetic events provides a unique opportunity to better understand the coupling nature between the solar wind-magnetosphere-ionosphere system. Cross wavelet analysis (XWT) exposes high common power regions between the solar wind velocity (Vsw) and interplanetary magnetic field component (IMF-Bz), plasma pressure (Psw), plasma density (Nsw), Geomagnetic Auroral Electrojet (AE) index and Symmetrical Ring Current Index (SYM-H). Another useful tool is wavelet transform coherence (WTC), which we have applied to measure how coherent the XWT is in time-frequency space. Thus, the local correlation between two continuous wavelet transforms (CWTs) can be conceived of as WTC. Moreover, we examined the relationship among the solar wind parameters during storm events using detrended cross-correlation analysis (DXA) with possible explanations. The study's findings will demonstrate that the suggested methods are a simple, effective, and robust method for gaining deeper insight into the complex spatiotemporal characteristics of time series.

Keywords: Interplanetary structures, Coronal Mass Ejections, Geomagnetic Storms, Magnetosphere, Cross Wavelet Transform, Wavelet Transform Coherence

Introduction

The solar wind is a large stream of plasma ejected by the Sun that extends outward from the corona and flows towards interplanetary space at an average speed of approximately 250 to 400 kms^{-1} (Parker, 1958). It brings a tremendous amount of kinetic and electrical energy through various solar activities such as Solar Flares (SFs), Coronal Mass Ejections (CMEs), and Corotating Interaction Regions (CIRs) (Tsurutani et al., 1992; Cane, 2000; Subedi et al., 2017; Silwal et al., 2021a). When some amount of these energies penetrates the Earth's magnetosphere, the electromagnetic and viscous forces cause a couple of these solar particles with the magnetosphere, supplying the system with momentum and energy (Poudel et al., 2019); these imported energies interrupt geomagnetic activity, causing geomagnetic storms, sub-storms, and aurora (Gonzalez et al., 1994).

Geomagnetic storms are extreme space weather activities that directly impact the ionosphere-atmosphere system, human technology, and life on Earth (Lastovicka, 2002). During the storm, the raised energy level from the magnetosphere to the upper atmosphere produces a substantial fluctuation in the F-region's electron density. It affects plasma distribution in the ionosphere environment by causing significant changes in magnetosphere convection currents (Chakraborty et al., 2015). Moreover, they significantly affect satellite systems, including radio communication satellites (Allen & Wilkinson, 1993). Variation in solar and geomagnetic activities significantly changes thermosphere mass density at the altitude of satellite operation, ultimately causing an impact on the drag effect of the satellite system and extra orbital decay (Li & Lei, 2021). Furthermore, over the auroral regions, storms generate currents to flow through electric power supplies and networks (Allen and Wilkinson, 1993). When the storm-generated geomagnetically induced current (GIC) is active in transformers, it causes half-cycle saturation of multiple transformers across the network at the same time, causing significant inductive voltage loading and harmonics in each of these transformers, exceeding the voltage control ability and protection limits of devices across vast areas of the network (Kappenman, 1996). In addition, past studies (e.g., Bochníček et al., 1999, 2001) show the geomagnetic storms are also associated with the weather; they observed that the distribution of pressure and temperature has a relationship with

solar and geomagnetic events, especially during very intense or very weak activities. Storms also greatly impact human health, affecting heart rate, arterial diastolic and systolic pressure, and behaviour of people, especially from lower and higher latitudes (Roederer, 1995; Papailiou, 2011). Other numerous studies (e.g., Palmer et al., 2006; Babayev & Allahverdiyeva, 2007; Mendoza & Sánchez de la Peña, 2010; Papailiou, 2011) have also shown the effect of solar activities on human health using different data analysis approaches.

The coupling of the solar wind with the Earth's magnetosphere and the coupling of magnetospheres with the ionosphere are the primary causes of geomagnetic field changes (Dungey, 1961). For the measurement of various geomagnetic disruptions that arise over short periods, geomagnetic indices are used. The Disturbance Storm-Time (Dst) index and the AE (auroral electrojet) index are the two major indices that are often used to monitor fluctuations of Earth's magnetic field strength (Sugiura, 1964; Rostoker, 1972). The Dst index represents the drop of the longitudinal mean magnetic field at lower latitudes, which is the most common approach to detect the strength of magnetic storms and magnetospheric ring current (Lundstedt et al., 2002). The Sun's activity governs the range of Dst value; however, the assumed range of Dst lies between +100 to -600 nT, where positive Dst signifies the contraction of magnetosphere because of solar wind pressure increment (Subedi et al. 2017). The separation between the top and bottom regions of the superposed H-component graphs from the magnetic observatories at the auroral zone is called the AE index (Kamide & Rostoker, 2004). It estimates the global electrojet activity in the auroral zone (Davis and Sugiura, 1966; Kivelson & Russel, 1995).

On the basis of Dst value, Gonzalez et al. (1994) classified geomagnetic storms into four categories: weak or small storm ($-50 < Dst \leq -30$nT), moderate storm ($-100 < Dst \leq -50$nT), intense storm ($-250 < Dst \leq -100$nT), and very intense storm (≤ -250 nT). Since SYM-H has the distinct advantage of having 1-min time resolution compared to the 1-hour time resolution of Dst, it is often used to identify the geomagnetic conditions based on the intensity of the storm time ring current. The onset of a geomagnetic storm involves a sudden positive increase in SYM-H value, termed as Sudden Storm Commencement (SSC). It is due to the shock wave created by the sudden increase in solar wind arriving on the Earth, which causes the sudden field increase (Perreault & Akasofu, 1978). Then, the elevated field does not change significantly for a certain period of time, referred to as the initial phase of the storm. When the enhanced solar stream reaches the Earth's

magnetosphere, it increases the number of energetic particles in the magnetosphere's trapping region, resulting in the increment of the ring current and hence causes the depression of SYM-H, which is referred to as the main phase (Gonzalez et al., 1999). When new particles are no longer injected, the ring currents decay slowly for one or two days. The excess particles are lost during this time, and the magnetic field gradually returns to its normal value. This period is referred to as the recovery phase, which normally lasts for a few hours to days depending upon the strength and interplanetary origin of the geomagnetic storm (Yokoyama & Kamide, 1997; Perreault & Akasofu, 1978).

Solar wind (SW) parameters and geomagnetic (GM) indices are essential indicators to look at while tracking and forecasting space weather events. Various studies have been conducted in the past to investigate the relationship between these parameters during storm events by employing a variety of mathematical methods such as autocorrelation, continuous wavelet analysis, and discrete wavelet analysis, amongst other techniques (e.g., Kane et al., 2005; Echer et al., 2008; Guo et al., 2010; Adhikari et al., 2018; Poudel et al., 2019; Silwal et al., 2021a). While there are a variety of statistical tools available, wavelet analysis has emerged as a particularly useful technique for investigating the local behaviour of geomagnetic disturbances caused by solar magnetic activity and their influence on solar wind parameters and geomagnetic indices during different phases of geomagnetic storms. From the physical point of view, this is an indication of the real meaning of this tool.

In this particular study, we intend to look at a relationship of solar wind velocity with other various SW parameters and GM indices during two different intense geomagnetic storm events using powerful statistical tools, XWT and WTC, along with DXA. This paper is structured as follows: Section 2 describes the data set, Section 3 specifies the methodology, Section 4 presents the findings with possible explanations, and Section 5 concludes this research work's findings.

1. Data Set

Different geomagnetic disturbances such as minor, moderate and severe conditions can be determined by analysing the National Oceanic and Atmospheric Administration (NOAA) scale. We have taken two intense events with different strengths and nature for this study. The geomagnetic indices, the symmetric horizontal component of the geomagnetic field (SYM-H) and auroral electrojet (AE), and SW parameters: southward interplanetary magnetic field (IMF-Bz),

proton speed (Vsw), proton density (Nsw), and pressure (Psw) were considered. The minute resolution data of previously mentioned parameters were downloaded from the OMNI Web Data Explorer system through the website: https://omniweb.gsfc.nasa.gov/form/omni_min.html. The detailed information about the studied events is presented in Table 1.

2. Methodology

In this section, the statistical tools and methods utilized in this study are described. We have applied wavelet analysis to study the variation characteristics of the SW parameters and GM indices during two different intense geomagnetic storms of consecutive SCs. In addition, the DXA was employed to study the correlation between two time series data and measure the degree of similarity between them.

2.1. Wavelet Transform Method

Most raw signals in the physical world are described in their time domain, and the graph representing them is simply a time amplitude representation of that signal. The analysis of signals is required to understand any physical mechanism, and analysing any signal also involves accessing information about the signal's frequency content and the time at which that frequency occurs. Various mathematical transformations have been developed as tools to process these signals and obtain additional essential information about them. The wavelet analysis is a powerful tool for analysing nonstationary signals and the localised oscillatory feature in time-frequency space (Torrence & Compo, 1998; Grinsted et al., 2004). The wavelet analysis is broadly categorised into two forms: Continuous Wavelet Transform (CWT) and Discrete Wavelet Transform (DWT). Particularly for extracting features, the Morlet wavelet (dimensionless frequency, ω_0 = 6) is an excellent choice due to its reasonable time and frequency localisation (Grinsted et al., 2004). The CWT is particularly effective at detecting localised and quasi-periodic variations in time series data (Li et al., 2005; Deng et al., 2013; Xie et al., 2017). The wavelet transform has been extended to include the XWT and WTC, which are nonlinear approaches that are commonly used to investigate the phase relationship between two time series in the time-frequency domain (Torrence & Compo, 1998; Grinsted et al., 2004). While the XWT spectrum reveals significant common power regions and relative phase between two time series in time-frequency space, the WTC spectrum quantifies the degree to which two time series co-vary as a

function of time and frequency (Li et al., 2009; Xiang & Kong, 2015; Deng et al., 2012). The XWT of two time series X (t) and Y (t) is defined as:

$$W_t^{XY}(s) = W_t^X(s)W_t^{Y*}(s) \quad (1)$$

Where, $W_t^X(s)$ and $W_t^Y(s)$ denote the CWT coefficients of sequence X (t) and Y (t) at frequency scale s, respectively and * represents the complex conjugate. The result of $W_t^{XY}(s)$ is complex, so the modulus $\|W_t^{XY}(s)\|$ indicates regions of high specific power in time-frequency space.

Because no normalisation with regard to the wavelet powers is performed in XWT, Maraun and Kurths (2004) noticed that the XWT could produce significant misleading results, i.e., the spectrum of one of the time series exhibits strong peaks, even though there is no relationship between the two time series. In order to address this problem, a normalised measure for the relationship between X (t) and Y (t) was provided, namely wavelet coherence (WTC), in which the XWT power is normalised by the spectrum of the two time series.

$$R_t\ (\mathrm{s}) = \frac{|W_t^{XY}(s)|}{\sqrt{W_t^X(s)\ W_t^{Y*}(s)}} \quad (2)$$

One can notice that the nominator and denominator of R_t (s) formulation can be equal if the spectrum is not calculated independently. As a result, some smoothing on the estimation of single and cross wavelet spectrums should be done in advance to estimate wavelet coherence (Torrence and Compo, 1998), as follows:

$$R_t^2(s) = \frac{|S[s^{-1}W_t^{XY}(s)]|^2}{S[s^{-1}W_t^X(s)]S[s^{-1}W_t^Y(s)]} \quad (3)$$

Here, S is the smoothing operator and is given by (Grinsted et al., 2004);

$$S(W) = S_{scale}(S_{time}(W_t^{XY}(s))) \quad (4)$$

Where, S_{scale} and S_{time}denote the smoothing along the wavelet scale axis and smoothing in time, respectively (Torrence & Compo, 1998; Grinsted et al., 2004; Maraun and Kurths, 2004). WTC values around 1 indicate a higher degree of resemblance across time series, whilst coherence values near 0 indicate no correlation (Boako & Alagidede, 2017).

In general, XWT can better expose common high-power time-frequency areas, while WTC is more effective at identifying time-frequency correlations even in areas where both time series have low powers (Maraun and Kurths, 2004).

Detrended Cross-Correlation Analysis (DXA)

Cross-correlation is a powerful tool for estimating statistical relationships between different variables as a function of time lag (Vichare et al., 2012). It is a technique of evaluating multiple parameters, which detects similarities and develops similar relative features and explores hidden information (Usoro, 2015; Poudel et al., 2020). The value of the correlation coefficient lies between -1 to +1. When the curve reaches ±1, it indicates a very strong correlation, and when it approaches around zero, it indicates a weak correlation (Katz, 1979; Karki et al., 2020).

To obtain insights into the mechanisms of natural processes, cross-correlation functions, including auto-correlation functions, are often used; these approaches should only be used in the context of stationarity, as per their definitions (Podobnik et al. 2009). Numerous time series of physical, biological, economic, and social systems, on the other hand, are nonstationary and have long-range power-law associations; because of these non-stationarities, statistical features of these systems are harder to analyse in practice (Podobnik et al. 2009). A revision of covariance analysis was performed by Podobnik (2007) in order to evaluate the long-range cross-correlations when non-stationeries are involved, called Detrended Cross-Correlation Analysis (DXA). We used DXA to examine the relationship of Vsw with SW parameters, Nsw, Psw, IMF-Bz, and GM indices, SYM-H and AE index, for our study. The lead or lag between the indices was determined using the time scale. The detailed explanation and mathematical expressions of DXA can be found in the papers, Podobnik (2007) and Podobnik et al. (2009).

3. Result and Discussion

In this section, we have described the observations and results of two different events. The geomagnetic activities were classified as minor, moderate, and severe conditions. These classifications were done based on the geomagnetic index, SYM-H, which was first provided by Kamide et al. (1998). The SYM-H index summarises the stages during a geomagnetic storm. In order to identify geomagnetic conditions based on the intensity of the storm time ring current, we

used SYM-H, which has the distinct advantage of having 1-min time resolution compared to the 1-hour time resolution of Dst.

4.1. Observed Geomagnetic Indices and Solar Wind Parameters

4.1.1. Event 1: 20 November 2003

The indicative study presented in Figure 1 represents variation in interplanetary parameters and geomagnetic indices during a super intense storm that occurred on 20 November 2003. It was triggered by the compression of a CME from active region 0501 on the solar disc, which afterwards grew into a MC (Gopalswamy et al., 2005). According to the reduction in the Dst index, it is the greatest storm in the solar cycle 23. Around 08:00 UT, the storm's first SSC occurred, marking the onset of the geomagnetic storm. This was followed by a prolonged main phase with the lowest SYM-H value of -490 nT at 18:17 UT. Then the recovery period began, lasting a few days.

It is clearly evident that when the magnetosphere is under quiet conditions, the solar wind parameters and geomagnetic indices do not show significant fluctuations, as indicated by their observed normal value before the storm. On the contrary, under the development of the storm, IMF-Bz suddenly changed its polarity to southward, reaching a value of -15 nT and -52 nT at ~08:09 UT and ~15:30 UT respectively, on the initial and main phase of the storm. A strongly negative Bz leads to magnetic reconnection, a principal means by which particles, energy and momentum are exchanged from solar wind to the Earth's Magnetosphere (Dungey, 1961). The plasma density (Nsw), flow speed (Vsw) and plasma pressure climbed sharply to 20 N/cc, 550 km/s and 14 nPa, respectively, around the initial phase of the storm at ~ 08:09 UT and then experienced a slight decrease, but again these parameters peaked with a maximum value of 30 N/cc, 766 km/s and 23 nPa, respectively, during the main phase of the storm. Quite similar behaviour was also shown by the AE index, by reaching a value of >2000 nT at two time periods, one at the initial phase and the other during the storm's main phase, but a slight lag of 10-20 minutes was noticed in AE index. The fact that a satellite cannot monitor ring current particles over the entire local time sector at any given moment explains why a lag between the apparent AE and other parameters was observed, especially during the storm's main phase. In accordance with Ahn et al.

(2002), the satellite was not in the same local time sector as the partial ring current, which develops mostly during the storm's main phase of development.

4.1.2. Event 2: 22 June 2015

Figure 2 represents the variation of the aforementioned interplanetary parameters and geomagnetic indices during an intense geomagnetic storm on 22 June 2015. Following the geomagnetic storm that occurred on St. Patrick's Day (17 March 2015), it was the second most powerful geomagnetic storm event in solar cycle-24. A pair of CMEs hit the Earth's magnetopause on 22 June 2015, at 5:45 UT and 18:35 UT, respectively, which were the primary cause of this storm event. As a consequence, the geomagnetic field activity ranged from quiet to severe storm conditions (Singh & Sripathi, 2017).

A tiny shock connected with the first CME was reported around 05:45 UT on 22 June 2015. IMF Bz increased from ~6 nT (northward) to ~ -10 nT (southward) during the shock period (upper panel of Figure 2), with a corresponding increase in solar wind speed from 350 km/s to 430 km/s and pressure reaching ~10 nPa. On the same day, the arrival of the second CME at 18:30 UT caused another shock, with considerable changes in interplanetary parameters. The positive shifting of the SYM-H index (88 nT) in the bottom panel of Figure 2 indicates that the second SSC happened at ~18:39 UT. During the storm's main phase, the value of SYM-H dropped to -139 nT at its lowest point, at about 20:17 UT. The Vsw grew abruptly from ~440 to ~718 km/s, Psw climbed from 5 to 59 nPa, and the IMF-Bz component suddenly shifted southern, reaching a low value of ~ -40 nT at 19:30 UT in undershielding conditions. Following that, the IMF Bz moved northward to nearly ~28 nT at 20:30 UT, reflecting the overshielding state; then, it steadily moved southward to ~17 nT, fluctuating between ±25 nT for 3–4 hours, from 21:00 to 23:59 UT.

Taking into account how these solar wind parameters influenced ground magnetic field observations, it is worth noting that while the first shock of CME had no effect on 22 June, the second shock of CME had an impact on the high and middle latitudes, where the AE index jumped from 500 nT to >2,000 T (second last panel of Figure 2) due to the enhanced of Chapman Ferraro currents in magnetopause (Singh & Sripathi, 2017). During the geomagnetic storm period, substorms can be triggered by fluctuations in the IMF and solar wind parameters (Nayar et al., 2006). This is justified by the intensification of the AE index, which is a primary indicator of magnetospheric substorm activity (Rostoker, 1972, Shadrina, 2017).

4.2. Cross wavelet transform (XWT) analysis

Here, we have presented the results of XWT obtained from CWTs of Vsw and the rest of the above-mentioned parameters. The horizontal axis represents time in hours (minutes data), and the vertical axis represents the period in minutes. The colours in the wavelet spectrum indicate the structure of common power regions, with the power range from weak (dark blue shades) to strong (red shades).

4.2.1. Event 1: 20 November 2003

Figure 3 portrays XWT between the Vsw and the aforementioned interplanetary parameters along with geomagnetic indices on the super intense geomagnetic storm of 20 November 2003. The XWT finds regions with high common power even in a noisy environment (Anusasananan, 2019; Prokoph & El Bilali, 2008). The common features associated with two time series are clearly identified in the wavelet power spectrum, such as the significant common fluctuations at around 8-9 hours, corresponding to the time of bow shock associated with the solar wind. All the analysed series also have high power in the 4 – 8, 8 - 16 and 16 - 32 minutes band on the storm day, as indicated by the thick black lines, which shows 5% significance level. The degree of resemblance between the portrayed patterns over this time period is relatively low, and it is thus hard to establish whether it is just a coincidence. This is when the cross-wavelet transform comes in handy (Grinsted et al., 2004).

4.2.2 Event 2: 22 June 2015

Figure 4 portrays XWT between the Vsw and the aforementioned interplanetary parameters along with geomagnetic indices on the super intense geomagnetic storm of 22 June 2015. As mentioned earlier, the XWT is calculated from the two CWTs, so it identifies regions of high common power between two physically related time series data.

The cross-wavelet power spectra between Vsw and geomagnetic indices, AE and SYM-H, show significant common power in the multiple bands, mostly at 4 - 64 minutes in the regions 18-20 hrs, remaining at 64 - 256 minutes in the regions 16 – 21 hrs. Similarly, for interplanetary/solar wind parameters, Vsw and IMF-Bz show high common power in lower bands, 4 - 16 minutes, in two different regions 18.50 – 20 hrs, and 20.28 – 21 hrs, and at higher bands, 64 - 256 minutes, in the regions 17 - 21 hrs, which resemble the time of initial and main phase of the storm. Also, the key periodicities associated with common power regions of Vsw and Nsw are observed at two different

bands, one at 4 - 32 minutes, which corresponds to the regions of initial phase time, and the other at 32 - 256 minutes in the regions that correspond to both initial and main phase time of the storm.

Similar patterns were also observed for Vsw and Psw. Also, the thick black lines clearly indicate the 5% significance level, and it is worth mentioning that the area of a time-frequency plot is a reliable measure of causality when the significance level is less than or equal to 5% (Grinsted et al., 2004, Damette & Goutte, 2020). Overall, the oscillations in solar wind velocity are manifested in the interplanetary and geomagnetic parameters, suggesting a significant period of coherence featured by co-movements in Vsw over these parameters. So, the shock associated with the CME that hits the Earth's Magnetosphere is evident in all of these parameters through XWT analysis.

4.3. Wavelet Transform Coherence (WTC) analysis

In this sub-section, we have presented the results of WTC between Vsw and the rest of the above mentioned interplanetary and geomagnetic parameters in order to measure how coherent is XWT in time-frequency space. WTC is a powerful statistical tool for analysing two time series nonlinear behaviour and determining significant coherence despite low common power. The WTC analysis can be used to determine the local correlation between two time series in time-frequency space (Grinsted et al., 2004; Deng et al., 2012; Xu et al., 2013). The time period is represented by the x-axis, while the y-axis shows the frequency or scale. The thick black contours show the 95% confidence level in the wavelet power spectrum using Monte Carlo simulations with a phase randomised surrogate series (Grinsted et al. 2004; Nie et al., 2020). In order to separate locations with reliable and less accurate estimations, a cone of influence (COI) (the dashed black line) is inserted where edge effects might distort the picture. The colour code for power spans from blue (low power) to red (high power). Arrows depict the relative phase relationship (in-phase pointing right, anti-phase pointing left) between two time series (Su et al., 2020). Using the WTC approach to examine two time series data (let's say X (t) and Y (t), arrows pointing NE and SW indicate that the X (t) is leading, while arrows pointing NW and SE indicate that the Y (t) is leading.

4.3.1. Event 1: 20 November 2003

Wavelet coherence between the Vsw and the aforementioned interplanetary parameters along with geomagnetic indices during the geomagnetic storm of 20 November 2003 is shown in Figure 5. The WTC approach is applied to explore and illustrate the co-movement between the studied parameters at different time-frequency (period) spaces. As mentioned before, the orientation of the

arrows indicates the level and type of correlation. The WTC spectrum in Figure 5 shows that WTC between Vsw and Psw, Nsw have a common significant region of above 95% confidence level at two scales, one at 2-64 minutes in the regions 6-9 hrs and the other at 32-64 minutes in the regions of 15-20 hrs. In these regions, they possess in-phase relationship.

On top of that, the Vsw and Psw show in-phase relation for the entire day at a larger scale, pointing to the fact that plasma pressure and flow speed are closely related to the entire period, i.e., from the onset of the geomagnetic storms to the recovery phases. On the other hand, results of the WTC between Vsw and IMF-Bz reveal that the power is extremely low, indicating that the two-time series does not have a similar significant region at timescales of a geomagnetically disturbed day. In light of this finding, we can infer that the fluctuation in IMF-Bz intensity during a storm is weakly related to the variation in solar wind velocity. Several early researchers have addressed the weak correlation between IMF-Bz and Vsw (e.g., Subedi et al., 2017; Silwal et al., 2021a) during few storm events.

Additionally, the local correlation of Vsw and geomagnetic indices was also investigated through WTC, and the result of WTC between Vsw and AE show that there was a common significant region in the scale of 64-128 minutes around 7-10 hrs with arrows pointing upward, indicating a lead of AE over Vsw by 90°. The leading phase refers to a wave that occurs "ahead" of another wave of the same frequency. Similarly, the results of WTC between Vsw and SYM-H show a common significant region at a timescale similar to that of AE. However, the phase of coherence is slightly different. The arrows point slightly to the right in the high-power spectrum region, indicating the in-phase relationship between them.

4.3.2. Event 2: 22 June 2015

Wavelet coherence between the Vsw and the aforementioned interplanetary parameters, along with geomagnetic indices during the geomagnetic storm of 22 June 2015, is shown in Figure 6. The WTC spectrum of Vsw and Psw, Nsw shows that during an intense geomagnetic storm of solar cycle 24, Vsw correlates strongly with Nsw and Psw, as indicated by the high-power spectrum in multiple bands, 64-256 minutes band for the entire observation period, 4-16 minutes around 4-6 hrs, 16-64 minutes around 4-8 hours and 32-64 minutes around 9-14 hrs. At these regions, the arrows point right, indicating the in-phase relationship between them.

In comparison to the geomagnetic storm of 20 November 2003, the results of WTC between Vsw and IMF-Bz in this event presented the strong local correlation between them at several bands, 4-16 minutes for almost the entire observation period, 16-32 minutes at around 2-6 hrs, 32-64 minutes at 8-11 hrs, 128-256 minutes at 12 hrs onward to the end of the day and 64-128 minutes at 15-20 hours with arrows pointing slightly to the left, indicating that the relationship between IMF-Bz and Vsw is negative during several phases of the storms. From the results of WTC based on two events, the potential relationship between Vsw and IMF-Bz may vary with the intensity and interplanetary causes of the geomagnetic storms.

Furthermore, the WTC of Vsw and geomagnetic indices for this event is quite similar to that of the 2003 event. A common significant region in the scale of 128-256 minutes around 15-21 hrs was seen in the WTC spectrum of Vsw and AE, with arrows pointing upward, indicating a lead of AE over Vsw by 90°. Similarly, the results of WTC between Vsw and SYM-H show a common significant region at the timescale of 64-128 minutes at 4-6 hrs and 48-256 minutes at 11-20 hrs. It is clearly evident that these periodicities are associated with two CME hit. The local correlation between Vsw and SYM-H is quite strong for this event. However, the phase of coherence is comparable to that of the earlier event. As we can see, the arrows are pointing slightly to the right, indicating that the relationship between Vsw and SYM-H is in phase during several phases of the storms.

From the analysis of WTC, the local correlation, time delay, and phase structure between the two-time series in time-frequency space can be explored. WTC finds locally phase-locked behavior, where XWT unveils high common power (Grinsted et al., 2004, Anusasananan, 2019, Nie et al., 2020). In prior research, two forms of wavelet analysis, i.e., many researchers widely used CWT and DWT (e.g., Nayar et al., 2006; Katsavrias et al., 2012; Silwal et al., 2021a; Mishra et al., 2021a) to localise the abrupt changes on the different parameters of space weather; however, the tools XWT and WTC show its great usefulness in order to track common powers on the multiple time series with its association (positive/negative) at the particular time frame. The time-frequency domain serves better visualisation of how one variable of space climate responds to another variable. These techniques were also used as a powerful statistical approach to study different solar phenomena (e.g., El-Borie et al., 2020; Ghaderpour et al., 2018; Marques de Souza et al., 2018; Kasde et al., 2014; Bolzan et al., 2012). Our results also presented these statistical tools as

extremely useful methods to study the short-term and long-term variation of the variables with their relationships.

4.4 Detrended Cross-Correlation Analysis (DXA)

The streams generated from various solar activities exhibit significant changes in all interplanetary variables, including Vsw, Nsw, and magnetic field strength (B), during the maximum speed period, signifying radially released strong shocks (Gerontidou et al., 2018). These noticeable changes can be observed from the significant variation in geomagnetic indices such as AE and SYM-H. In Figure 7, we tried to look at the relationship between solar wind parameters and geomagnetic indices using the DXA approach. Figure 7 shows that solar wind speed is associated with other solar wind parameters and geomagnetic indices during geomagnetic storm events at different time lead/lag. Figures 7(left) and 7(right) represent the detrended cross-correlation analysis of Vsw with IMF-Bz (blue line), Nsw (orange line), Psw (yellow line), AE (purple line), and SYM-H (green line) during the geomagnetic storm events of 20 November 2003, and 22 June 2015, respectively. For DXA, we have used minutes resolution data of the event day. The x-axis depicts the time in minutes, which lies from -1440 to +1440, and the y-axis shows the value of the cross-correlation coefficient, which ranges from -1 to +1.

During the event of 20 November 2003, Vsw was found to be negatively correlated with Bz and SYM-H with a correlation coefficient of -0.70 and -0.71 at a time lag of 240 and 460 minutes, respectively. The positive association of Vsw was observed with Psw and AE at 0 and 20 minutes lag with the correlation coefficient of +0.63 and +0.54, respectively. However, a moderate relationship was observed for Vsw with Nsw; the plot finds the maximum value of cross-correlation coefficient as +0.36 at 485 minutes time lag. On the other hand, during the storm event of 22 June 2015, Vsw was found to be positively correlated with Bz, Nsw, and Psw at time lags of 70, 2, and 0 minutes with correlation coefficients +0.66, +0.88, and +0.95, respectively. The correlation of Vsw and SYM-H was negative, with a correlation coefficient of -0.72 at a time lag of 58 minutes. Vsw showed its different relationship with AE at different time lags; however, the maximum correlation coefficient was observed at 186 minutes time lag with a correlation coefficient of 0.59. The correlation coefficients and time lead/lag between various solar wind parameters during the studied geomagnetic storms period can also be observed in Table 2.

In order to establish the relationship between two time series data, traditional correlation analysis was widely used in this field (e.g., Köhnlein, 1996; Marques de Souza et al., 2018; Silwal et al., 2021b; Mishra et al., 2021b). However, we presented detrended cross-correlation analysis, which is extremely useful for the study of long-term power-law relationships as it can handle the data with non-stationaries. DXA clearly presented the association between two time series data with better visualisation of time lead or lag on the relationship between the signals.

We used the DXA and WT analysis to detect the key periods of fluctuations associated with the solar wind parameters and geomagnetic indices. It is evident from Figures 3-6 that the results obtained using the two approaches are quite encouraging. This short-term oscillation of the interplanetary plasma parameters and geomagnetic indices appears to be caused by the periodic oscillation of the solar wind. Nevertheless, various studies (e.g., Webb & Howard, 1994; Owens & Crooker, 2006; Smith et al., 2013) indicate that the time-varying component of these parameters is related to the corresponding flux expelled by CMEs. Furthermore, McIntosh et al. (2015) discovered that the magnetic surges from the activity bands, which exhibit a quasi-periodicity on short timeframes, are responsible for a wide range of energetic phenomena, including flares, solar wind, and CMEs. Consequently, we conclude that the quasi-periodicity of magnetic surges on the solar surface is a more credible explanation for these short-term periods of solar wind and IMF features than the alternative explanation proposed thus far.

Conclusion

Solar wind parameters and geomagnetic indices are key parameters for tracking and forecasting space weather activities. In the present work, we performed an analysis to derive the potential relationship between solar wind parameters and geomagnetic indices during the two strong geomagnetic storm events. We elaborated on the usefulness of three statistical tools, DXA, XWT, and WTC, to study the IP and geomagnetic features associated with the solar wind. The major findings obtained from this work are summarised below:

- From XWT analysis, the high common power regions in wavelet spectrums with common periodicities of 4 – 8, 8 - 16 and 16 - 32 minutes among solar wind velocity and other interplanetary parameters, Nsw, Psw along with geomagnetic indices, AE and SYM-H were identified in the case of super intense geomagnetic storm of 20 November 2003. In contrast, for the intense geomagnetic storms of 15 June 2015, XWT revealed the key

periodicities at almost all bands (4-256 minutes), corresponding to the regions of different phases of the storm. Thus, XWT analysis provides a comprehensive background for understanding the short-term variation of solar wind data during geomagnetic storm events.

- From WTC analysis, the coherency of XWT analysis was identified, and the potential relationship between solar wind velocity (Vsw) and other interplanetary parameters, Nsw, Psw and geomagnetic indices, AE, and SYM-H, was uncovered. For both events, Vsw possesses in-phase relationship with all the above-mentioned parameters except for the interplanetary magnetic field component, IMF-Bz. The potential relationship between Vsw and interplanetary magnetic field component, IMF-Bz, varied with the intensity and interplanetary causes of the geomagnetic storms.
- The detrended cross-correlation analysis (DXA) was used to look at the relationship of solar wind speed (Vsw) with solar wind density (Nsw), pressure (Psw), z-component of magnetic field (Bz), SYM-H and AE indices. For the geomagnetic event of 20 November 2003, Vsw was positively correlated with Psw, AE, and Nsw at a different time lead/lags with correlation coefficients of more than 0.54; however, it showed a negative association with Bz and SYM-H. Moreover, for the event 22 June 2015, Vsw shows a strong positive correlation with Bz, Nsw, AE and Psw with correlation coefficients greater than 0.66. Vsw showed a negative relationship with SYM-H. Different time lead/lag features were observed in the correlation of Vsw with AE during this event. Although DXA has been demonstrated to be an effective way for establishing correlations between SW parameters and GM indices, it overestimated the association between Vsw and IMF-Bz. This is where WTC comes in handy, as it uses Monte Carlo simulations to precisely assess the significance level in the wavelet spectrum. WTC discovered a weak correlation between Vsw and IMF-Bz, reshaping our understanding of the interaction between SW parameters and GM indices during severe space weather activities.

Through the present work, it has been shown that the newly developed tools, XWT, WTC, and DXA, are simple, effective and robust methods for studying the periodicity of fluctuation of solar wind and IMF features and identifying the correlation between them. The result ensures that it has a unique advantage over another analytical method to acquire a deeper insight into the complex spatiotemporal characteristics of any time series data. Overall, XWT and WTC results point to the fact that these approaches provide an alternative way of assessing the global effects of a

geomagnetic storm and could be used as a sophisticated tool to forecast the emergence of these unique events by tracking short and long term variations in the solar wind parameters and relative deviations in geomagnetic indices. However, the present study dealt with just two geomagnetic events over a global scale. Additional investigations involving additional events and local magnetic stations would be required to conduct a thorough analysis.

Author's Contribution

The authors S. P. Gautam and A. Silwal have developed the idea of this manuscript. The overall manuscript was prepared by them. They have a major contribution in all the sections, including computational and data analysis parts. P. Poudel and M. Karki have worked on the introduction and methodology section; they have also handled grammatical errors and plagiarism. This work was conducted under the regular guidance of the research advisors of the group N. P. Chapagain and B. Adhikari.

Acknowledgement

The data of interplanetary parameters and geomagnetic indices are extracted from the OmniWeb service: (http://omniweb.gsfc.nasa.gov/ow_min.html). We want to thank NASA for making the data available. Some of our software contains code that C. Torrence and G. Compo originally wrote; we are thankful to them.

Data availability: All the datasets and code used in this work can be obtained from https://doi.org/10.5281/zenodo.5167361.

Conflict of Interest: The authors declare that they have no conflict of interest.

Funding: This study was conducted under self-funding.

Ethical approval: Not applicable.

References

Adamowski, J. F. (2008). Development of a short-term river flood forecasting method for snowmelt driven floods based on wavelet and cross-wavelet analysis. *Journal of Hydrology*, *353*(3-4), 247–266. https://doi.org/10.1016/j.jhydrol.2008.02.013

Adhikari, B., Dahal, S., Sapkota, N., Baruwal, P., Bhattarai, B., Khanal, K., & Chapagain, N. P. (2018). Field-Aligned Current and Polar Cap Potential and Geomagnetic Disturbances: A Review of Cross-Correlation Analysis. *Earth and Space Science*, *5*(9), 440-455. https://doi.org/10.1029/2018EA000392

Ahn, B. H., Moon, G. H., Sun, W., Akasofu, S. I., Chen, G. X., & Park, Y. D. (2002). Universal time variation of the Dst index and the relationship between the cumulative AL and Dst indices during geomagnetic storms. *Journal of Geophysical Research: Space Physics*, *107*(A11), SMP-38. https://doi.org/10.1029/2002JA009257

Allen, J. H., Wilkinson, D. C. (1993). Solar-terrestrial activity affecting systems in space and on Earth. Solar-Terrestrial Predictions—IV. In: Hruska, J., et al. (Eds.), NOAA=ERL, Boulder, pp. 75 –107.

Anusasananan, P. (2019, November). Wavelet spectrum analysis of PM10 data in Bangkok, Thailand. *In Journal of Physics: Conference Series*, *1380*(1), 012017. https://doi.org/10.1088/1742-6596/1380/1/012017

Babayev, E. S., & Allahverdiyeva, A. A. (2007). Effects of geomagnetic activity variations on the physiological and psychological state of functionally healthy humans: Some results of Azerbaijani studies. *Advances in Space Research*, *40*(12), 1941–1951. https://doi.org/10.1016/j.asr.2007.02.099

Bishop, M. P., Young, B. W., Huo, D., & Chi, Z. (2020). Spatial Analysis and Modeling in Geomorphology. *Reference Module in Earth Systems and Environmental Sciences*, pp. 1–32. https://doi.org/10.1016/b978-0-12-409548-9.12429-7

Boako, G. & Alagidede, P. (2017). Co-movement of Africa's equity markets: Regional and global analysis in the frequency–time domains. *Physica A: Statistical Mechanics and Its Applications*, *468*, 359–380. https://doi.org/10.1016/j.physa.2016.10.088

Bochníček, J., Hejda, P. & Pýcha, J. (2001). Comparison of Solar and Geomagnetic Activity Effects on the Northern Hemisphere Weather Changes. *Studia Geophysica et Geodaetica*, *45*, 133–154. https://doi.org/10.1023/A:1021812210921

Bochníček, J., Hejda, P., Bucha, V., & Pýcha, J. (1999). Possible geomagnetic activity effects on weather. *Annales Geophysicae*, *17*(7), 925–932. https://doi.org/10.1007/s00585-999-0925-4

Bolzan, M. J., Echer, E., & Korth, A. (2012). Cross-wavelet analysis on the interplanetary and magnetospheric tail magnetic field data. In Congresso Nacional de Matemática Aplicada e Computacional (SBMAC), vol. 34, pp. 797-802.

Cane, H. V. (2000). Coronal mass ejections and Forbush decreases. *Cosmic rays and Earth*, 55-77. https://doi.org/10.1007/978-94-017-1187-6_4

Chakraborty, M., Kumar, S., De, B. K., & Guha, A. (2015). Effects of geomagnetic storm on low latitude ionospheric total electron content: A case study from Indian sector. *Journal of Earth System Science*, *124*(5), 1115–1126. https://doi.org/10.1007/s12040-015-0588-3

Damette, O. & Goutte, S. (2020). Weather, pollution and Covid-19 spread: a time series and Wavelet reassessment, halshs-02629139f, available online: https://halshs.archives-ouvertes.fr/halshs-02629139/

Davis, T. N., & Sugiura, M. (1966). Auroral electrojet activity index AE and its universal time variations. *Journal of Geophysical Research*, *71*(3), 785-801. https://doi.org/10.1029/JZ071i003p00785

Debnath, L. (2003). Wavelet transforms and their applications. *Applications of Mathematics*, *24*(1), 395–457. https://doi.org/10.5860/choice.39-6472

Domingues, M. O., Mendes Jr, O., & da Costa, A. M. (2005). On wavelet techniques in atmospheric sciences. *Advances in Space Research*, *35*(5), 831-842. https://doi.org/10.1016/j.asr.2005.02.097

Dungey, J. W. (1961). Interplanetary magnetic field and the auroral zones. *Physical Review Letters*, *6*(2), 47. https://doi.org/10.1103/PhysRevLett.6.47

Echer, E., Gonzalez, W. D., & Tsurutani, B. T. (2008). Interplanetary conditions leading to superintense geomagnetic storms (Dst≤− 250 nT) during solar cycle 23. *Geophysical Research Letters*, *35*(6). https://doi.org/10.1029/2007GL031755

El-Borie, M. A., El-Taher, A. M., Thabet, A. A., & Bishara, A. A. (2020). The interconnection between the periodicities of solar wind parameters based on the interplanetary magnetic field polarity (1967–2018): a cross wavelet analysis. *Solar Physics*, *295*(9), 1-20. https://doi.org/10.1007/s11207-020-01692-2

Gerontidou, M., Mavromichalaki, H., & Daglis, T. (2018). High-speed solar wind streams and geomagnetic storms during solar cycle 24. *Solar Physics*, *293*(9), 1-18. https://doi.org/10.1007/s11207-018-1348-8

Ghaderpour, E., Ince, E. S., & Pagiatakis, S. D. (2018). Least-squares cross-wavelet analysis and its applications in geophysical time series. *Journal of Geodesy*, *92*(10), 1223-1236. https://doi.org/10.1007/s00190-018-1156-9

Gonzalez, W. D., Josely, J. A., Kamide, Y., Korehi, H. W., Rostoker, G., Tsuruntani, B. T., & Vasylianas, V. M. (1994). What is a geomagnetic storm? *Journal of Geophysical Research*, *99*, 5771–5792. https://doi.org/10.1029/93JA02867

Gopalswamy, N., Yashiro, S., Michalek, G., Xie, H., Lepping, R. P., & Howard, R. A. (2005). Solar source of the largest geomagnetic storm of cycle 23. *Geophysical research letters*, *32*(12). https://doi.org/10.1029/2004GL021639

Goupillaud, P., Grossmann, A., & Morlet, J. (1984). Cycle-octave and related transforms in seismic signal analysis. *Geoexploration*, *23*(1), 85-102. https://doi.org/10.1016/0016-7142(84)90025-5

Grinsted, A., Moore, J. C. & Jeverejeve, S. (2004). Application of the cross wavelet transform and wavelet coherence to geophysical time series. *Nonlinear Processes in Geophysics*, *11*(4), 515–533. https://doi.org/10.5194/npg-11-561-2004. https://doi.org/10.5194/npg-11-561-2004

Grossmann, A. and Morlet, J. (1984). Decomposition of Hardy Functions into Square Integrable Wavelets of Constant Shape. *SIAM Journal on Mathematical Analysis*, *15*(4), 723-736. https://doi.org/10.1137/0515056.

Guo, J., Feng, X., Forbes, J. M., Lei, J., Zhang, J., & Tan, C. (2010). On the relationship between thermosphere density and solar wind parameters during intense geomagnetic storms. *Journal of Geophysical Research: Space Physics*, *115*(A12). https://doi.org/10.1029/2010JA015971

Habibi, A. (1995). Introduction to wavelets. Proceedings - IEEE Military Communications Conference MILCOM, vol. 2, pp. 50–61. https://doi.org/10.1201/b18057-6

Köhnlein, W. (1996). Cross-correlation of solar wind parameters with sunspots ('Long-term variations') at 1 AU during cycles 21 and 22. *Astrophysics and Space Science*, *245*(1), 81-88.

Kamide, Y., & Rostoker, G. (2004). What is the physical meaning of the AE index? *Eos, Transactions American Geophysical Union*, *85*(19), 188. https://doi.org/10.1029/2004EO190010

Kamide, Y., Baumjohann, W., Daglis, I. A., Gonzalez, W. D., Grande, M., Joselyn, J. A., ... & Vasyliunas, V. M. (1998). Current understanding of magnetic storms: Storm-substorm relationships. *Journal of Geophysical Research: Space Physics*, *103*(A8), 17705-17728. https://doi.org/10.1029/98JA01426

Kane, R. P. (2005). How good is the relationship of solar and interplanetary plasma parameters with geomagnetic storms?. *Journal of Geophysical Research: Space Physics*, *110*(A2). https://doi.org/10.1029/2004JA010799

Kappenman, J. G. (1996). Geomagnetic Storms and Their Impact on Power Systems. *IEEE Power Engineering Review*, *16*(5), 5. https://doi.org/10.1109/MPER.1996.491910

Karki, M., Silwal, A., Chapagain, N. P., Poudel, P., Gautam, S. P., Mishra, R. K., ... & Orue, Y. O. M. (2020). GPS Observations of Ionospheric TEC Variations during 2015 Mw 7.8 Nepal Earthquake. *Earth and Space Science Open Archive ESSOAr*, Preprint. https://doi.org/10.1002/essoar.10504866.1

Kasde, S. K., Gwal, A. K., & Sondhiya, D. K. (2014). Application of Cross Wavelet Transform and Wavelet coherence to sunspot area and sunspot number during the ascending phase of solar cycle 24. *40th COSPAR Scientific Assembly*, *40*, D2-2.

Katsavrias, C., Preka-Papadema, P., & Moussas, X. (2012). Wavelet analysis on solar wind parameters and geomagnetic indices. *Solar Physics*, *280*(2), 623-640. https://doi.org/10.1007/s11207-012-0078-6

Katz, R. W. (1988). Use of cross-correlation in the search for teleconnections. *Journal of the Royal Meteorological Society*, *8*, 241–253. https://doi.org/10.1002/joc.3370080303

Kivelson, M. G., Russel, C. T. Introduction to Space Physics. Cambridge University Press, (1995). https://doi.org/10.1017/9781139878296

Labat, D. (2010). Cross wavelet analyses of annual continental freshwater discharge and selected climate indices. *Journal of Hydrology*, *385*, 269–278. https://doi.org/10.1016/j.jhydrol.2010.02.029

Lastovicka, J. (2002). Monitoring and forecasting of ionospheric space weather--effects of geomagnetic storms. *Journal of Atmospheric and Solar-Terrestrial Physics*, *64*, 697 –705. https://doi.org/10.1016/S1364-6826(02)00031-7

Li, R., & Lei, J. (2021). The determination of satellite orbital decay from POD data during geomagnetic storms. *Space Weather*, *19*, e2020SW002664. https://doi.org/10.1029/2020SW002664

Lundstedt, H., Gleisner, H., & Wintoft, P. (2002). Operational forecasts of the geomagnetic Dst index. *Geophysical Research Letters*, *29*(24), 34-1. https://doi.org/10.1029/2002GL016151

Marques de Souza, A., Echer, E., Bolzan, M. J. A., & Hajra, R. (2018). Cross-correlation and cross-wavelet analyses of the solar wind IMF B z and auroral electrojet index AE coupling during HILDCAAs. *In Annales Geophysicae*, *36*(1), 205-211. Copernicus GmbH. https://doi.org/10.5194/angeo-36-205-2018

McIntosh, S. W., Leamon, R. J., Krista, L. D., Title, A. M., Hudson, H. S., Riley, P., ... & Ulrich, R. K. (2015). The solar magnetic activity band interaction and instabilities that shape quasi-periodic variability. *Nature Communications*, *6*(1), 1-11. https://doi.org/10.1038/ncomms7491

Mendoza, B., & Sánchez de la Peña, S. (2010). Solar activity and human health at middle and low geomagnetic latitudes in Central America. *Advances in Space Research*, *46*(4), 449–459. https://doi.org/10.1016/j.asr.2009.06.021

Mishra, R. K., Gautam, A., Poudel, P, Parajuli, N., Silwal, A., Adhikari, B., Tiwari, B. R., Gautam, S. P. (2021). Geomagnetically Quiet Period analysis of Relativistic Electrons, Auroral Precipitation, Joule Heating, and Ring Current during the Years of 1999, 2000 and 2004. *Journal of Nepal Physical Society*, *7*(2), 126-137.

Mishra, R. K., Silwal, A., Baral, R., Adhikari, B., Braga, C. R., Gautam, S. P., ... & Migoya-Orue, Y. (2021). Singularity Detection on Forbush Decrease at High Latitude Stations During Geomagnetic Disturbances, ResearchSquare, Preprint. https://doi.org/10.21203/rs.3.rs-324774/v1

Navarro, L., Courbebaisse, G., & Jourlin, M. (2014). Logarithmic wavelets. *Advances in imaging and electron physics*, *183*, 41-98. https://doi.org/10.1016/B978-0-12-800265-0.00002-3

Nayar, S. R. P., Radhika, V. N., & Seena, P. T. (2006, February). Investigation of substorms during geomagnetic storms using wavelet techniques. In *Proceedings of the ILWS Workshop Goa*, India pp. 19-24.

Nie, Y., Chen, P., Zhang, T., & Wang, E. (2020). Impacts of international oil price fluctuations on China's PM2. 5 concentrations: a wavelet analysis. *Economic research-Ekonomska istraživanja*, *33*(1), 2488-2508. https://doi.org/10.1080/1331677X.2019.1656098

Owens, M. J., & Crooker, N. U. (2006). Coronal mass ejections and magnetic flux buildup in the heliosphere. *Journal of Geophysical Research: Space Physics*, *111*(A10). https://doi.org/10.1029/2006JA011641

Palmer, S.J., Rycroft, M.J. & Cermack, M. (2006). Solar and geomagnetic activity, extremely low frequency magnetic and electric fields and human health at the Earth's surface. *Surv Geophys*, *27*, 557–595. https://doi.org/10.1007/s10712-006-9010-7

Papailiou, M., Mavromichalaki, H., Kudela, K., Stetiarova, J., & Dimitrova, S. (2011). Effect of geomagnetic disturbances on physiological parameters: An investigation on aviators. *Advances in Space Research*, *48*(9), 1545–1550. https://doi.org/10.1016/j.asr.2011.07.004

Parker, E. N. (1959). Dynamics of the interplanetary gas and magnetic fields. *Astrophysical Journal*, *128*, 664. https://doi.org/10.1086/146579

Perreault, P., & Akasofu, S. I. (1978). A study of geomagnetic storms. *Geophysical Journal International*, *54*(3), 547-573. https://doi.org/10.1111/j.1365-246X.1978.tb05494.x

Podobnik, B., & Stanley, H. E. (2008). Detrended cross-correlation analysis: a new method for analysing two nonstationary time series. *Physical review letters*, *100*(8), 084102. https://doi.org/10.1103/PhysRevLett.100.084102

Podobnik, B., Grosse, I., Horvatić, D., Ilic, S., Ivanov, P. C., & Stanley, H. E. (2009). Quantifying cross-correlations using local and global detrending approaches. *The European Physical Journal B, 71*(2), 243–250. https://doi.org/10.1140/epjb/e2009-00310-5

Poudel, P., Parajuli, N., Gautam, A., Sapkota, D., Adhikari, H., Adhikari, B., ... & Mishra, R. K. (2020). Wavelet and Cross-Correlation Analysis of Relativistic Electron Flux with Sunspot Number, Solar Flux, and Solar Wind Parameters. *Journal of Nepal Physical Society, 6*(2), 104-112. https://doi.org/10.3126/jnphyssoc.v6i2.34865

Poudel, P., Simkhada, S., Adhikari, B., Sharma, D., & Nakarmi, J. J. (2019). Variation of solar wind parameters along with the understanding of energy dynamics within the magnetospheric system during geomagnetic disturbances. *Earth and Space Science, 6,* 276–293. https://doi.org/10.1029/2018EA000495

Prokoph, A., El Bilali, H. (2008). Cross-Wavelet Analysis: a Tool for Detection of Relationships between Paleoclimate Proxy Records. *Math Geosci., 40*, 575–586. https://doi.org/10.1007/s11004-008-9170-8

Roederer, J. G. (1995). Are magnetic storms hazardous to your health?. Eos, Transactions *American Geophysical Union, 76*(44), 441-445. https://doi.org/10.1029/95EO00273

Rostoker, G. (1972). Geomagnetic indices. *Reviews of Geophysics, 10*(4), 935-950. https://doi.org/10.1029/RG010i004p00935

Shadrina, L. P. (2017). Two types of geomagnetic storms and relationship between Dst and AE indexes. In *E3S Web of Conferences* (Vol. 20, p. 01010). EDP Sciences. https://doi.org/10.1051/e3sconf/20172001010

Silwal, Ashok. (2021). Data and Code for "Study of Solar Wind and Interplanetary Magnetic Field Features Associated with Geomagnetic Storms: The Cross Wavelet Approach" (1.0.0) [Data set]. Zenodo. https://doi.org/10.5281/zenodo.5167361

Silwal, A., Gautam, S. P., Chaudhary, K., Khanal, M., Joshi, S., Dangaura, S., & Adhikari, B. (2021a). Study of Solar Wind Parameters During Geomagnetic Storm of 26 August 2018 and 28 September 2017. *Thai Journal of Physics, 38*(2), 54-68.

Silwal, A., Gautam, S. P., Poudel, P., Karki, M., Adhikari, B., Chapagain, N. P., ... & Migoya-Orue, Y. (2021b). Global positioning system observations of ionospheric total electron content variations during the 15 January 2010 and 21 June 2020 solar eclipse. *Radio Science*, *56*(5), 1-20. https://doi.org/10.1029/2020RS007215

Singh, R., & Sripathi, S. (2017). Ionospheric response to 22–23 June 2015 storm as investigated using ground-based ionosondes and GPS receivers over India. *Journal of Geophysical Research: Space Physics*, *122*(11), 11-645. https://doi.org/10.1002/2017JA024460

Smith, C. W., Schwadron, N. A., & DeForest, C. E. (2013). Decline and recovery of the interplanetary magnetic field during the protracted solar minimum. *The Astrophysical Journal*, *775*(1), 59. https://doi.org/10.1088/0004-637X/775/1/59

Su, W., Wu, X., Geng, X., Zhao, X., Liu, Q., & Liu, T. (2019). The short-term effects of air pollutants on influenza-like illness in Jinan, China. *BMC public health*, *19*(1), 1-12. https://doi.org/10.1186/s12889-019-7607-2

Subedi, A., Adhikari, B., Mishra, R. K (2017). Variation of solar wind parameters during intense geomagnetic Storms. *Himalayan Physics*, *6 & 7*, 80-85. https://doi.org/10.3126/hj.v6i0.18366

Sugiura, M. (1964). Hourly values of equatorial Dst for the IGY. *Ann. Int. Geophys. Year*, *35*, 9.

Torrence, C. & Compo, G. P. (1998). A Practical Guide to Wavelet Analysis. *Bulletin of the American Meteorological Society*, *79*(1), 69–78. https://doi.org/10.1175/1520-0477(1998)079<0061:APGTWA>2.0.CO;2

Tsurutani, B. T., Gonzalez, W. D., Tang, F., & Lee, Y. T. (1992). Great magnetic storms. *Geophysical Research Letters*, *19*(1), 73-76. https://doi.org/10.1029/91GL02783

Usoro, A. E. (2015). Some basic properties of cross-correlation functions of n-dimensional vector time series. *Journal of Statistical and Econometric Methods*, *4*(1), 63–71

Vichare, G., Alex, S., & Lakhina, G. S. (2005). Some characteristics of intense geomagnetic storms and their energy budget. *Journal of Geophysical Research*, *110*, A03204. https://doi.org/10.1029/2004JA010418

Webb, D. F., & Howard, R. A. (1994). The solar cycle variation of coronal mass ejections and the solar wind mass flux. *Journal of Geophysical Research: Space Physics*, *99*(A3), 4201-4220. https://doi.org/10.1029/93JA02742

Xu, W. H., Xing, Z. Y., Balan, N., Liang, L. K., Wang, Y. L., Zhang, Q. H., ... & Li, W. B. (2021). Spectral analysis of geomagnetically induced current and local magnetic field during the 17 March 2013 geomagnetic storm. *ResearchSquare*, *March*, 1–18. https://doi.org/10.21203/rs.3.rs-342899/v1

Yokoyama, N., & Kamide, Y. (1997). Statistical nature of geomagnetic storms. *Journal of Geophysical Research: Space Physics*, *102*(A7), 14215–14222. https://doi.org/10.1029/97JA00903

Yu, H. L. & Lin, Y. C. (2015). Analysis of space–time nonstationary patterns of rainfall–groundwater interactions by integrating empirical orthogonal function and cross wavelet transform methods. *Journal of* Hydrology, 525, 585-597. https://doi.org/10.1016/j.jhydrol.2015.03.057

Yu, L., & Wang, J. Q. (2014). Analysis of the Concentration of Pollutants Based on Wavelet Analysis. In *Applied Mechanics and Materials*, *575*, 566-569. https://doi.org/10.4028/www.scientific.net/AMM.575.566

Maraun, D., & Kurths, J. (2004). Cross wavelet analysis: significance testing and pitfalls. *Nonlinear Processes in Geophysics*, *11*(4), 505-514.

Gonzalez, W. D., Tsurutani, B. T., & De Gonzalez, A. L. C. (1999). Interplanetary origin of geomagnetic storms. *Space Science Reviews*, *88* (3), 529-562. https://doi.org/10.1023/A:1005160129098

Supporting Information

Contents:

Figures 1 to 7 and Tables 1 to 2

Introduction

This supporting information provides the tables and images with caption of the main article.

Table 1: Information of the geomagnetic storm events.

Events	***Date***	***Type***	***Minimum SYM-H value***	***Cause***
Event 1	20 Nov 2003	Super Intense	-490 nT	Compression of a CME, later evolved into a magnetic cloud (MC)
Event 2	22 June 2015	Intense	-139 nT	CMEs

Table 2: Cross-correlation coefficients and time lead/lag of Vsw and other solar wind parameters & geomagnetic indices during different geomagnetic storm events.

Correlating Parameters	*20 Nov 2003*		*22 June 2015*	
	Coeff.	Lead (+)/Lag (-) (Minutes)	Coeff.	Lead (+)/Lag (-) (Minutes)
Vsw - Bz	-0.70	-240	+0.66	-70
Vsw - Nsw	-0.36	-485	+0.88	+2
Vsw - Psw	+0.63	0	+0.95	0
Vsw - AE	+0.54	+20	-0.72	-58
Vsw - SYM-H	-0.71	-460	-0.59	-186

Figure 1. From top to bottom, the panels show the variation of the south-north component of Interplanetary magnetic field IMF-Bz (nT) in GSM coordinate system, plasma flow speed Vsw (km/s) and solar wind dynamic pressure Psw (nPa) (right), plasma density Nsw (n/cc), AE (nT) and SYM-H (nT) index with time (UT), respectively during the geomagnetic storm of 20 November 2003.

Figure 2. From top to bottom, the panels show the variation of the south-north component of Interplanetary magnetic field IMF-Bz (nT) in GSM coordinate system, plasma flow speed Vsw (km/s) and solar wind dynamic pressure Psw (nPa) (right), plasma density Nsw (n/cc), AE (nT) and SYM-H (nT) index with time (UT), respectively during the geomagnetic storm of 22 June 2015.

Figure 3. XWT between solar wind velocity (Vsw) and interplanetary parameters, IMF-Bz (a), Nsw (b), Psw (c) and geomagnetic indices, AE (d) and SYM-H (e) on 20 November 2003.

Figure 4: XWT between solar wind velocity (Vsw) and interplanetary parameters, IMF-Bz (a), Nsw (b), Psw (c) and geomagnetic indices, AE (d) and SYM-H (e) on 22 June 2015.

Figure 5: WTC between solar wind velocity (Vsw) and interplanetary parameters, IMF-Bz (a), Nsw (b), Psw (c) and geomagnetic indices, AE (d) and SYM-H (e) on 20 November 2003.

Figure 6: WTC between solar wind velocity (Vsw) and interplanetary parameters, IMF-Bz (a), Nsw (b), Psw (c) and geomagnetic indices, AE (d) and SYM-H (e) on 22 June 2015.

Figure 7: DXA of solar wind speed (Vsw) with density (Nsw), pressure (Psw), a southward component of interplanetary magnetic field (Bz), and geomagnetic indices, AE and SYM-H during the geomagnetic storm event of 20 November 2003 (left) and 22 June 2015 (right).

Figure 1

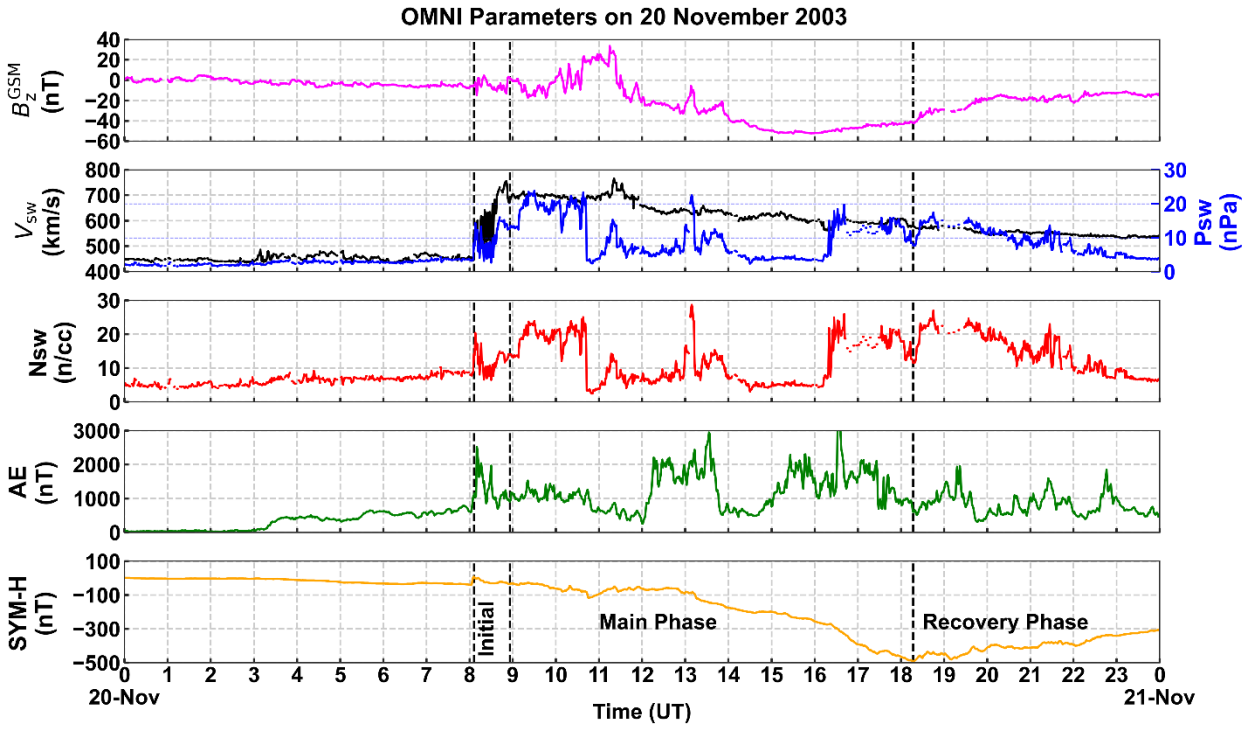
OMNI Parameters on 20 November 2003
B_Z^{GSM} (nT)
V_{sw} (km/s)
Psw (nPa)
Nsw (n/cc)
AE (nT)
SYM-H (nT)
Initial
Main Phase
Recovery Phase
20-Nov
21-Nov
Time (UT)

Figure 2

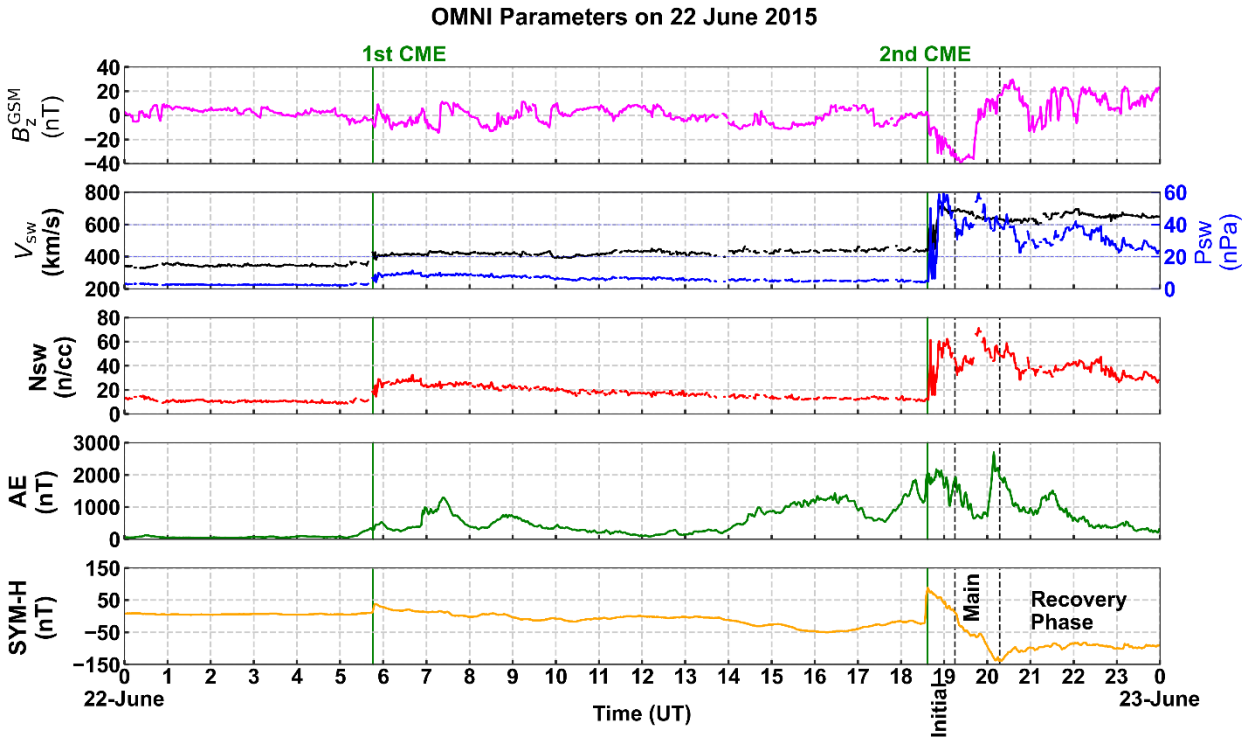
OMNI Parameters on 22 June 2015
1st CME
2nd CME
B_z^{GSM} (nT)
V_{sw} (km/s)
Psw (nPa)
Nsw (n/cc)
AE (nT)
SYM-H (nT)
Initial
Main
Recovery Phase
22-June
23-June
Time (UT)

Figure 3

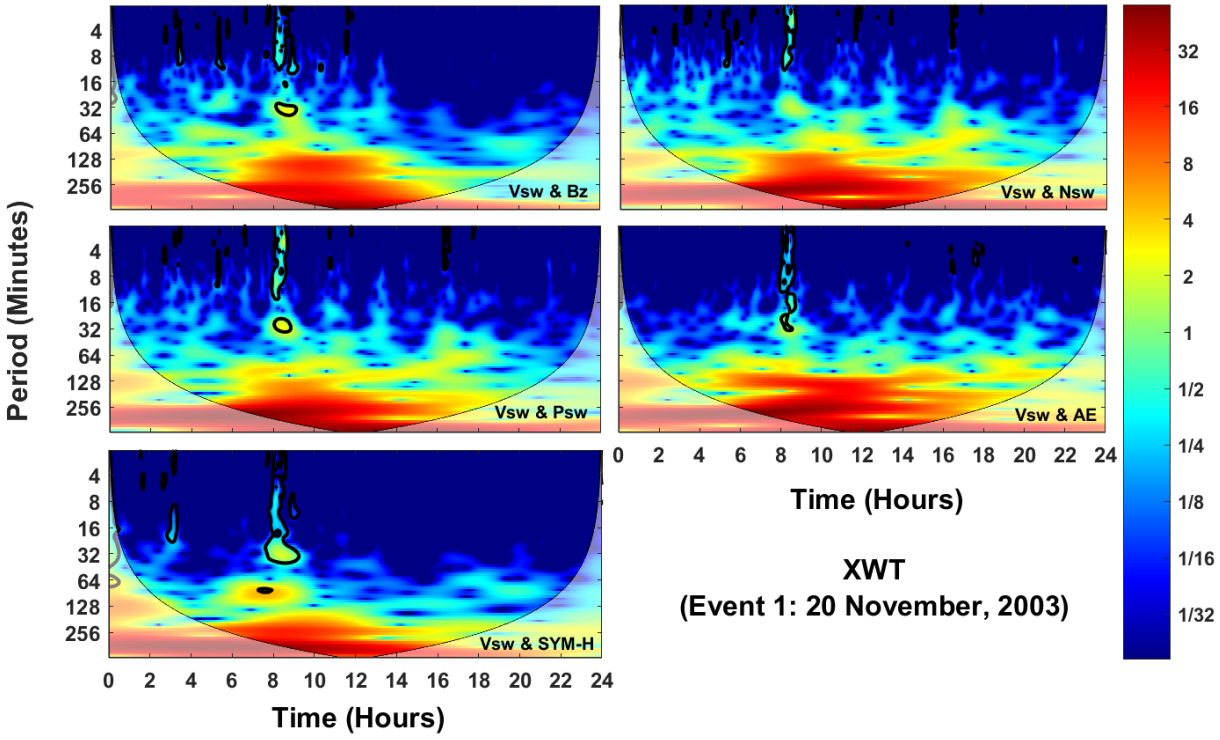
Period (Minutes)
4
8
16
32
64
128
256
Vsw & Bz
Vsw & Nsw
Vsw & Psw
Vsw & AE
Vsw & SYM-H
0 2 4 6 8 10 12 14 16 18 20 22 24
Time (Hours)
XWT
(Event 1: 20 November, 2003)
32
16
8
4
2
1
1/2
1/4
1/8
1/16
1/32

Figure 4

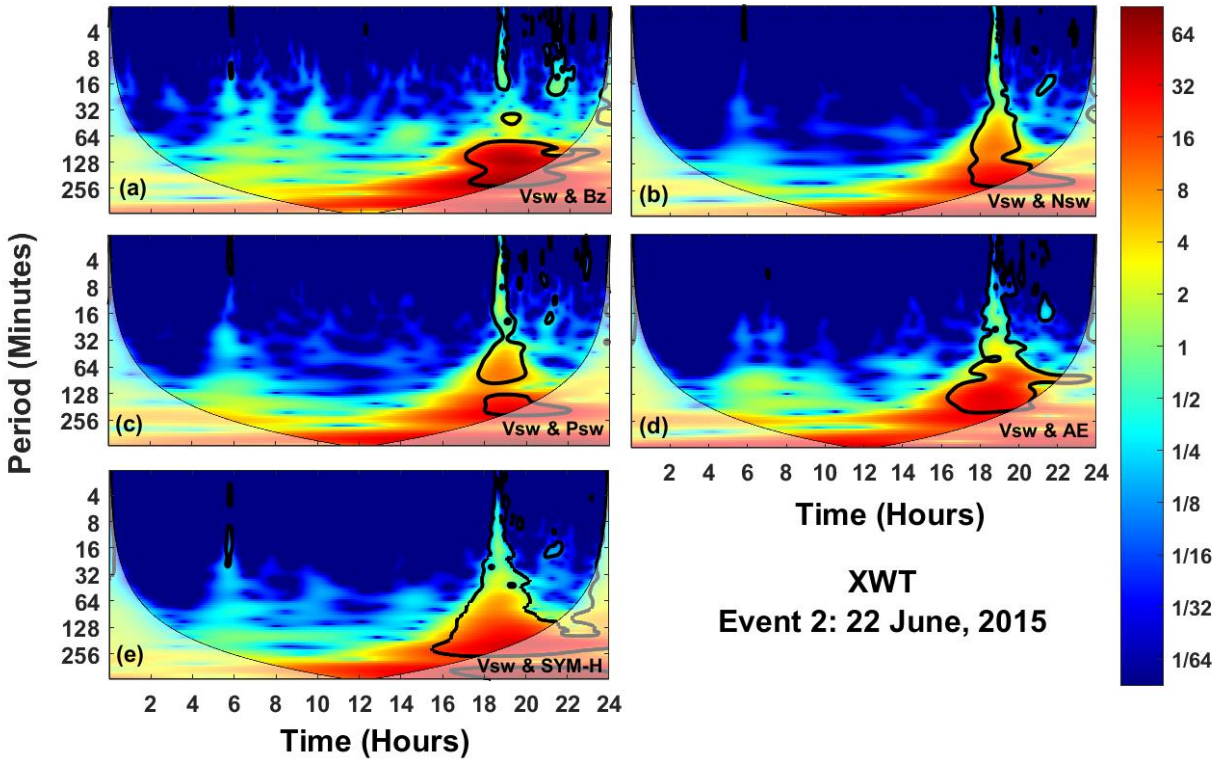
Period (Minutes)
4
8
16
32
64
128
256
(a)
Vsw & Bz
(b)
Vsw & Nsw
(c)
Vsw & Psw
(d)
Vsw & AE
(e)
Vsw & SYM-H
2 4 6 8 10 12 14 16 18 20 22 24
Time (Hours)
XWT
Event 2: 22 June, 2015
64
32
16
8
4
2
1
1/2
1/4
1/8
1/16
1/32
1/64

Figure 5

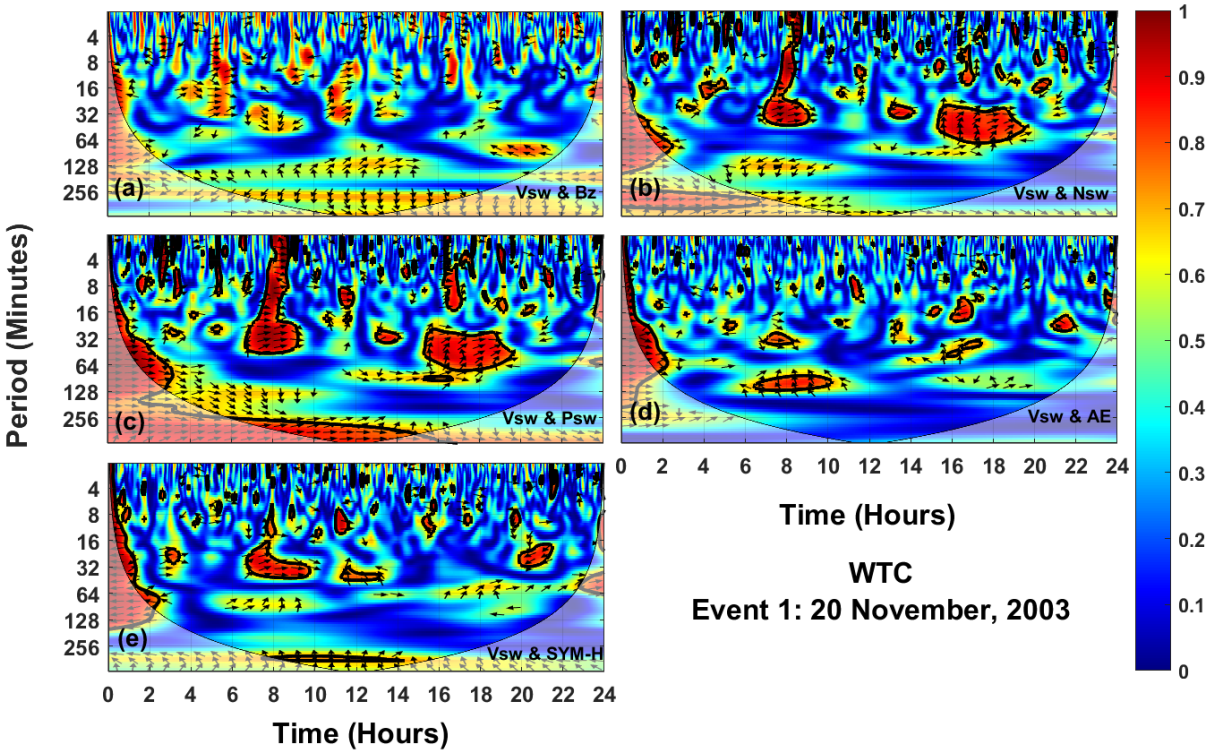
Period (Minutes)
4
8
16
32
64
128
256
(a)
Vsw & Bz
(b)
Vsw & Nsw
(c)
Vsw & Psw
(d)
Vsw & AE
(e)
Vsw & SYM-H
0 2 4 6 8 10 12 14 16 18 20 22 24
Time (Hours)
WTC
Event 1: 20 November, 2003
1
0.9
0.8
0.7
0.6
0.5
0.4
0.3
0.2
0.1
0

Figure 6

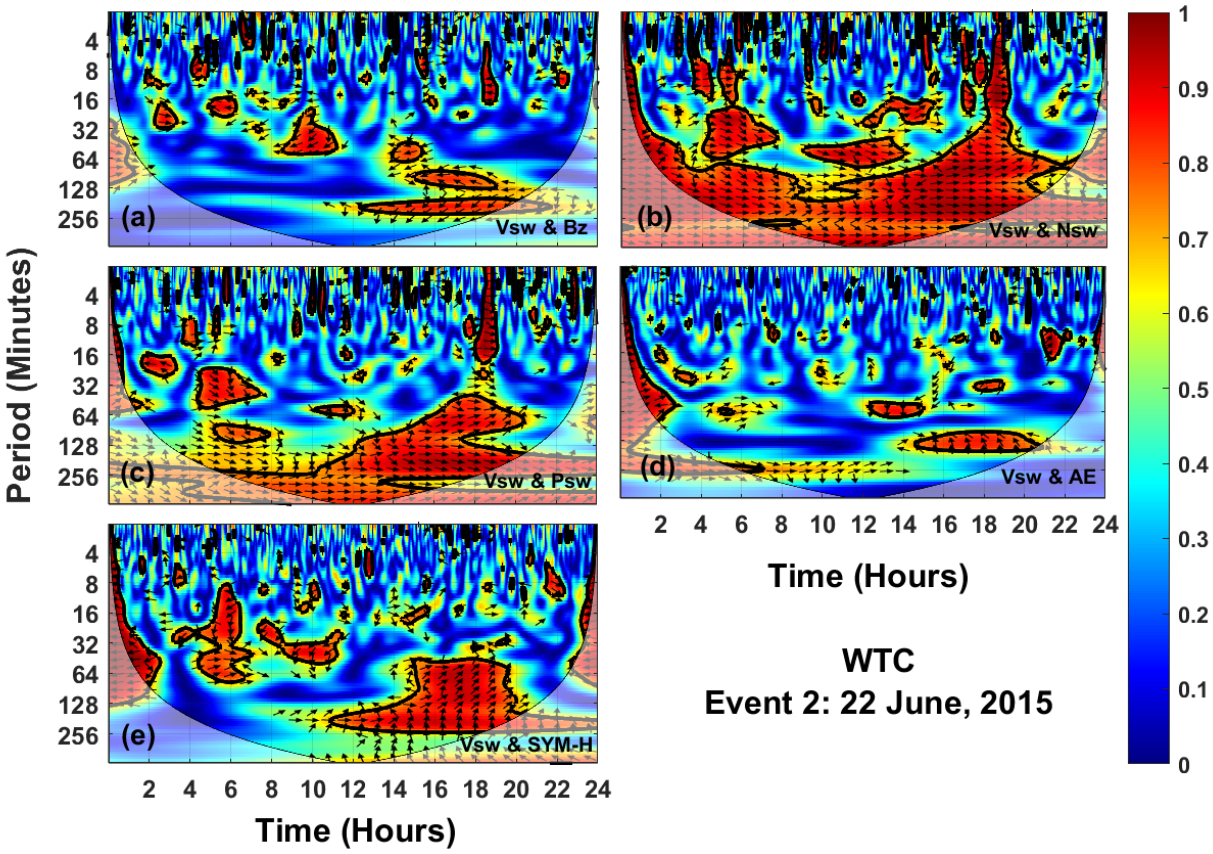
Period (Minutes)
4
8
16
32
64
128
256
(a)
Vsw & Bz
(b)
Vsw & Nsw
(c)
Vsw & Psw
(d)
Vsw & AE
(e)
Vsw & SYM-H
2 4 6 8 10 12 14 16 18 20 22 24
Time (Hours)
WTC
Event 2: 22 June, 2015
1
0.9
0.8
0.7
0.6
0.5
0.4
0.3
0.2
0.1
0

Figure 7 (left)

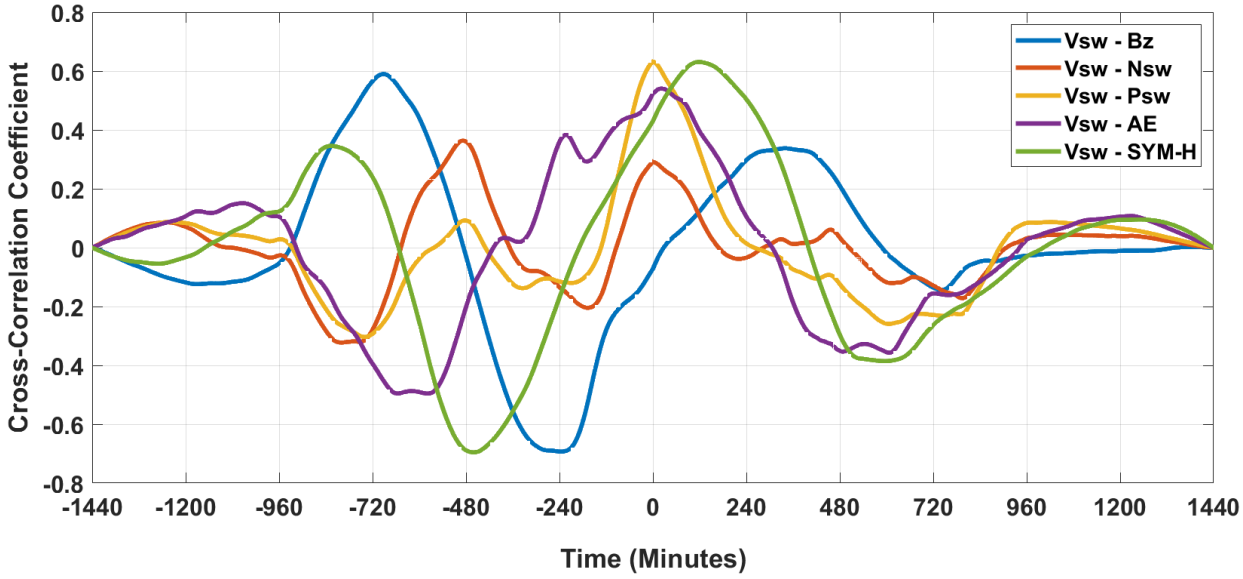

Figure 7 (right)